Supporting Information

Enhanced n-Doping Efficiency of a Naphthalenediimide-based Copolymer through Polar Side Chains for Organic Thermoelectrics

David Kiefer[†], *Alexander Giovannitti*[‡], *Hengda Sun*[§], *Till Biskup*[⊥], *Anna Hofmann*[†], *Marten Koopmans*[‖], *Camila Cendra*[#], *Stefan Weber*[⊥], *L. Jan Anton Koster*[‖], *Eva Olsson*[▽], *Jonathan Rivnay*[○], *Simone Fabiano*[§], *Iain McCulloch*[‡◊], *and Christian Müller*[†]*

[†] Department of Chemistry and Chemical Engineering, Chalmers University of Technology, 412 96 Göteborg, Sweden

[‡] Department of Chemistry and Centre for Plastic Electronics, Imperial College London, London SW7 2AZ, United Kingdom

[§] Laboratory of Organic Electronics, Department of Science and Technology, Linköping University, 602 21 Norrköping, Sweden

[⊥] Institut für Physikalische Chemie, Albert-Ludwigs-Universität Freiburg, 79104 Freiburg, Germany

[‖] Zernike Institute for Advanced Materials, 9747, AG, Groningen, The Netherlands

[#] Department of Materials Science and Engineering, Stanford University, Stanford CA 94304, United States

[▽] Department of Physics, Chalmers University of Technology, 412 96 Göteborg, Sweden

[○] Department of Biomedical Engineering, Northwestern University, Evanston IL 60035, United States

[◊] SPERC, King Abdullah University of Science and Technology, Thuwal 23955-6900, Saudi Arabia

Corresponding Author* christian.muller@chalmers.se

Experimental Section

Materials. p(gNDI-gT2) with a maximum length of n = 7 repeating units (cf. Figure S1) was synthesized according to a modified procedure of the previously published synthesis.[1] In the same study the ionization potential (IP) and electron affinity (EA) of the polymer was measured to be 4.8 eV and 4.1 eV, respectively. p(NDI2OD-T2) (M_n ~ 30 kg mol^{-1} and PDI ~ 2.1; Polyera ActivInk N2200) was purchased from Polyera Corp. and used as received. 4-(2,3-Dihydro-1,3-dimethyl-1H-benzimidazol-2-yl)-N,N-dimethylbenzenamine (N-DMBI; 98% - HPLC) was purchased from Sigma Aldrich and used as received. Chloroform ($CHCl_3$; purity > 99 %) was purchased from Fisher Scientific.

Sample fabrication. p(gNDI-gT2) and N-DMBI were freshly dissolved at 30 °C and concentrations of 10 g L^{-1} and 5 g L^{-1} in $CHCl_3$. Appropriate amounts of the N-DMBI solution were added to the p(gNDI-gT2) solution and subsequently spin-coated (1000 rpm for 45 s) on glass-slides with and without pre-patterned electrical contacts, Silicon substrates and PET substrates. p(NDI2OD-T2) was dissolved in o-dichlorobenzene at a concentration of 5 g L^{-1}, and the solution was stirred at 70 °C for about one hour to allow complete dissolution of the polymer. Doping was done by mixing with specific amounts of 5 g L^{-1} N-DMBI in o-dichlorobenzene solution. After stirring, the mixed solution was spin-coated onto the glass and subsequently thermally annealed at 110 °C under nitrogen atmosphere for 10 min. The sample preparation for electrical measurements was done in an N_2-filled glovebox; all other samples were prepared in air.

UV-vis absorption spectroscopy. Absorption measurements of liquid and solid samples were performed at room temperature with a PerkinElmer Lambda 900 spectrophotometer.

Electrical characterization. Electrical conductivity and Seebeck coefficient measurements were performed inside a nitrogen-filled glovebox using a semiconductor parameter analyzer

(Keithley 4200-SCS). All samples were annealed at 80 °C for 10 minutes in an N_2-filled glovebox prior to measuring the electrical conductivity and Seebeck coefficient. For electrical conductivity measurements and Seebeck measurements substrates with thermally evaporated 15 nm thick gold electrodes on a 3 nm thick Ti adhesion layer (length 15 mm, width 0.5 mm, channel width 1 mm) were used. The samples were fixed in between a pair of Peltier modules to maintain the desired temperature difference, and the thermal gradient ΔT was determined by of thermocouples on the sample surface. The electrical conductivity and Seebeck coefficient of the samples were measured by recording I-V curves without an applied temperature difference and by means of the shift of the I-V curves as a result of the thermovoltage $\Delta V = \Delta T\, S$. Measurements of the air stability of doped p(gNDI-gT2) were performed on substrates with gold electrodes with a channel length of 1000 μm and a channel width of 30 μm. I-V curves of the samples were first measured in an N_2 atmosphere and at different times after transfer to ambient atmosphere. Subsequently, the samples were returned to N_2 atmosphere and I-V curves were recorded before and after annealing at 80 °C for 10 minutes. Cryogenic measurements were conducted inside a cryogenic probe station manufactured by Janis Research. Liquid nitrogen was used for temperature control in joint with the heater inside the probe station.

Electron paramagnetic resonance (EPR) spectroscopy. Samples were prepared by spin coating ~100 nm thin films on uncoated PET substrates, which were cut to the appropriate size (3 x 0.3 mm). Spectra were recorded with a commercial spectrometer (Bruker EMX) using an X-band microwave bridge (Bruker ER 041 MR) and a high-quality cavity (Bruker 4119HS-W1) in conjunction with the respective acquisition software (Bruker 32-bit WIN-EPR Acquisition Version 3.0). The microwave frequency was read out from an external microwave frequency counter (Systron Donner 6520 Microwave Counter). The magnetic field has been calibrated using a Li:LiF standard with known g-factor. Spin counting was done by

comparing with standard samples with known number of spins (Bruker Strong Pitch and Weak Pitch) according to standard procedures. The thickness of films for EPR was measured with a KLA Tencor AlphaStep D-100 profilometer. Concentration of paramagnetic species in pristine p(gNDI-gT2) was below the detection limit of our setup, thus preventing extraction of spin density from the EPR spectra from this sample.

Atomic force microscopy (AFM). Topography images were obtained from spin-coated samples on Si-substrates with a Dimension Icon (Bruker) in Peak Force QNM mode using silicon cantilevers (ScanAsyst-Air) with a typical tip radius of approx. 2 nm, a spring constant of 0.4 N m^{-1} and a cantilever resonance frequency of about 70 kHz.

Transmission electron microscopy (TEM). Samples were prepared by spin-coating thin films on poly(3,4-ethylene dioxythiophene):poly(styrene sulfonate) PEDOT:PSS, followed by floating off films in water and finally collecting them on a TEM copper mesh grids. TEM images were recorded with a G2 T20 Tecnai transmission electron microscope operated at an acceleration voltage of 200 kV.

Scanning electron microscopy (SEM). Samples were prepared by spin coating films on cleaned Si/SiO_2 substrates and electron microscope images were acquired with a JEOL JSM-7800F Prime Field Emission Electron Microscope using an acceleration voltage of 1.5 kV. Note, that the samples did not require the application of any conducting coating.

Grazing-incidence wide-angle X-ray scattering (GIWAXS). Films were prepared by spinning on Si/SiO_2; samples were annealed in a glove box environment at 80 °C for 10 min. X-ray scattering was performed at the Stanford Synchrotron Radiation Lightsource (SSRL) on beam line 11-3 (2D scattering with an area detector, Rayonix MAR-225, at grazing incidence) with incident energy of 12.73 keV. The incidence angle (0.1°**)** was slightly larger than the critical angle, ensuring that we sampled the full depth of the film. The distance between

sample and detector was calibrated using a LaB6 polycrystalline standard. Raw data was normalized by monitor counts, and reduced and analyzed using a combination of Nika 1D SAXS[2] and WAXStools[3] software packages in Igor Pro. Here, q_{xy} (q_z) is the component of the scattering vector parallel (perpendicular) to the substrate.

Synthesis of p(gNDI-gT2)

The protocol for the synthesis of p(gNDI-gT2) reported in [1] was modified to increase the yield of the polymerization from 21 % to 94 %. The modification includes a change of the solvent from chlorobenzene to DMF and lowering the temperatures to 85 °C.

A 25 mL Schlenk tube was dried and purged with argon. gNDI-Br_2 (232.9 mg 0.25 mmol) and (3,3'-bis(2-(2-(2-methoxyethoxy)ethoxy)ethoxy)-[2,2'-bithiophene]-5,5'-diyl)bis-(trimethylstannane) (206.5 mg, 0.25 mmol), $Pd_2(dba)_3$ (4.6 mg, 5.1 µmol) and P(*o*-tol)$_3$ (6.2 mg, 20.0 µmol) were dissolved in 12 mL of anhydrous, degassed DMF. The reaction mixture was degassed for 10 min and heated to 85 °C for 4 h. After 4 hours, the end capping procedure was carried out. Then, the polymer was cooled to room temperature and the reaction mixture was precipitated in ethyl acetate, followed by the addition of hexane. The polymer was collected in a Soxhlet thimble and Soxhlet extraction was carried out with ethyl acetate, acetone, hexane, THF and chloroform. The polymer was dissolved in hot chloroform and the solution was concentrated *in vacuo* and precipitated in ethyl acetate, followed by the addition of hexane. Finally, the polymer was collected and dried under high vacuum for 16 h. A dark green polymer was obtained with a yield of 94 % (297 mg, 24.0 µmol).

^{1}H NMR (TFA-d_1, 400 MHz) δ: 8.93 (s, 2 H), 7.36 (s, 2H), 4.57 – 4.41 (m, 8H), 4.41 (s, 4H), 4.26 – 4.01 (m, 18H), 3.96 – 3.74 (m, 30H), 3.51 (s, 6H), 3.48 (s, 6H) ppm.

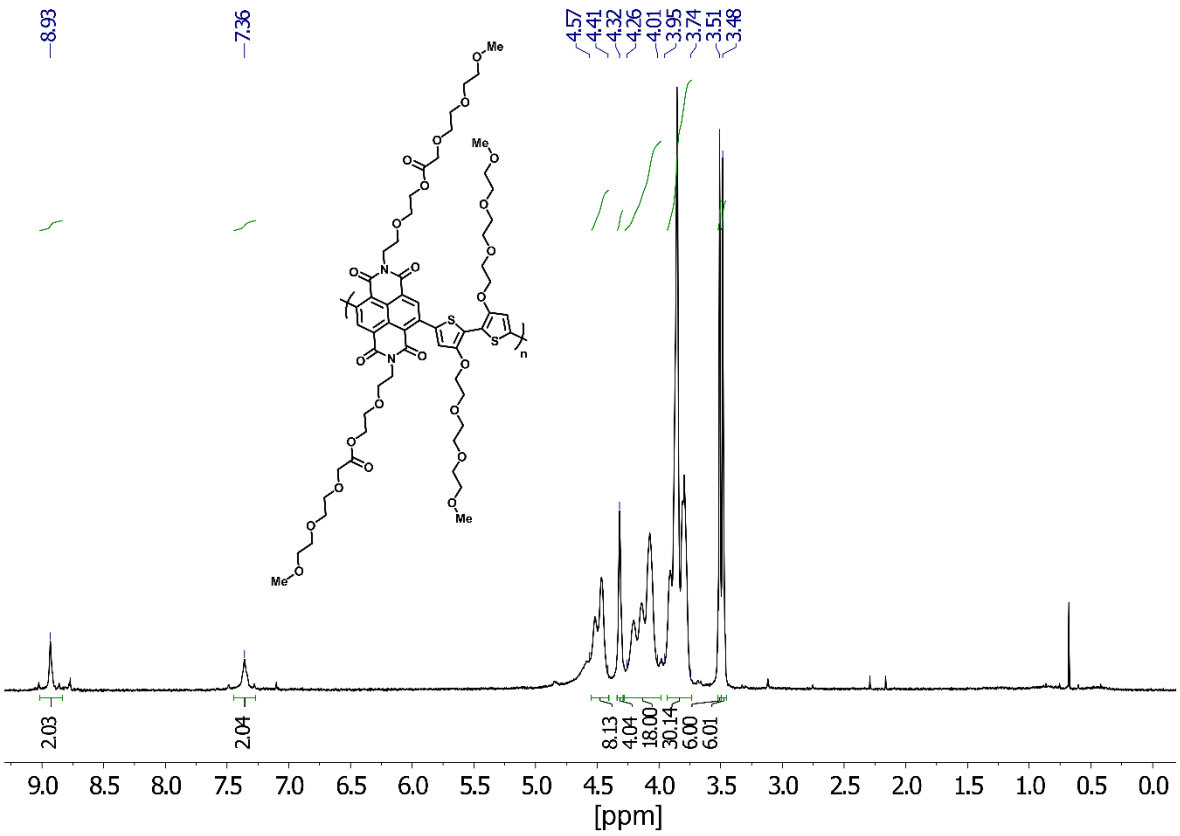

Figure S1. ^{1}H NMR spectrum of p(gNDI-gT2) in TFA-d_1. The copolymer is also soluble in $CDCl_3$, however the solvent peak of chloroform overlaps with the protons of the bithiophene and therefore the spectrum is reported in TFA-d_1.

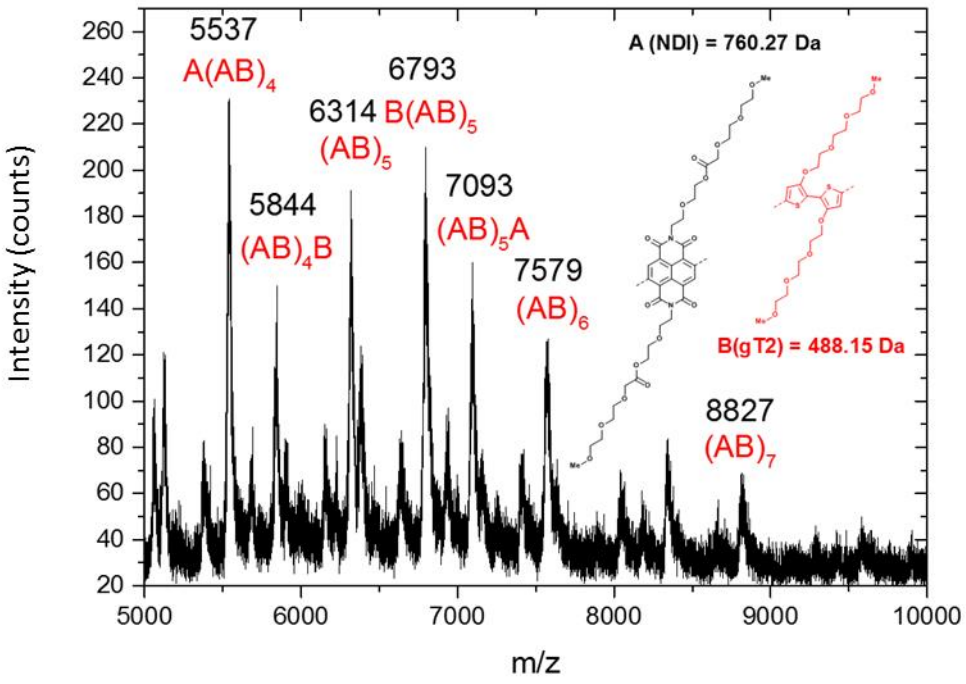

Figure S2. MALDI ToF of p(gNDI-gT2)

Table S1. Compiled literature values of the maximum electrical conductivity (σ_{max}) at the corresponding dopant molar fractions of n-doped organic semiconductors.

Semiconductor	**Dopant**	$\boldsymbol{\sigma_{max}}$ (S/cm)	$\boldsymbol{\alpha}$ **at** $\boldsymbol{\sigma_{max}}$ (μV K^{-1})	$\boldsymbol{\alpha^2\sigma}$ **at** $\boldsymbol{\sigma_{max}}$ (μW m^{-1}K^{-2})	**mol% at** $\boldsymbol{\sigma_{max}}$	**Reference**
p(gNDI-gT2)	N-DMBI	2.9×10^{-1}	-93	4.1×10^{-1}	20	This work
p(gNDI-gT2)	N-DMBI	1.1×10^{-1}	-190	2.5×10^{-1}	10	This work
P(NDI2OD-T2)	N-DMBI	6.8×10^{-4}	-502	1.7×10^{-2}	25	This work
x-PNDI-1TH	N-DMBI	4.0×10^{-5}			37	[4]
P(NDI2OD-T2)	2-Cyc-DMBI-H	3.4×10^{-4}			53	[5]
P(NDI2OD-T2)	$(2\text{-Cyc-DMBI})_2$	2.8×10^{-3}			11	[5]
P(NDI2OD-T2)	$(2\text{-Fc-DMBI})_2$	7.6×10^{-5}			26	[5]
P(NDI2OD-T2)	$(2\text{-Rc-DMBI})_2$	3.0×10^{-3}			12	[5]
P(NDI2OD-T2)	N-DMBI	8.0×10^{-3}	-850	5.8×10^{-1}	9	[6]
P(NDI2OD-T2)	N-DPBI	4.0×10^{-3}	-770	2.4×10^{-1}	9	[6]
P(NDI2OD-T2)	N-DPBI	1.0×10^{-3}			16	[7]
P(NDI2OD-TET)	N-DPBI	2.7×10^{-7}			10	[7]
P(PDI2OD-A)	$(2\text{-Cyc-DMBI})_2$	4.5×10^{-1}			43	[8]
P(PDI2OD-DEBT)	$(2\text{-Cyc-DMBI})_2$	7.0×10^{-2}			35	[8]
P(PDI2OD-T2)	$(2\text{-Cyc-DMBI})_2$	1.0×10^{-3}			35	[8]
P(PDI2OD-E)	$(2\text{-Cyc-DMBI})_2$	2.1×10^{-3}			32	[8]
P(NDI2OD-T2)	$(2\text{-Cyc-DMBI})_2$	4.0×10^{-3}			19	[8]
P(NDI2OD-T2)	$(RuCp^*Mes)_2$	4.0×10^{-3}			5	[9]
P(NDI2OD-T2)	[RhCp*Cp]	9.5×10^{-5}			1	[10]
P(NDI2OD-T2)	TDAE	5.0×10^{-3}	-150	1.1×10^{-2}	NA[a]	[11]
NTCDI2DT-2T	Na-SG	1.0×10^{-3}			NA[a]	[12]
NTCDI-AF4A	Na-SG	1.0×10^{-3}			NA[a]	[12]
PNDTI-BBT-DT	N-DMBI	1.8×10^{-1}	-56	5.6×10^{-2}	33	[13]
PNDTI-BBT-DP	N-DMBI	5.0×10^{0}	-169	1.4×10^{1}	33	[13]
PNDTI-BBT-DP	N-DMBI	1.2×10^{0}	-207	5.1×10^{0}	24[b]	[13]
BDPPV	N-DMBI	2.6×10^{-1}	-323	2.7×10^{0}	40	[14]
BDPPV	N-DMBI	4.8×10^{-2}	-650	2.0×10^{0}	24[b]	[14]
CIBDPPV	N-DMBI	5.3×10^{0}	-172	1.6×10^{1}	28	[14]
CIBDPPV	N-DMBI	3.5×10^{0}	-221	1.8×10^{1}	24[b]	[14]
CIBDPPV	N-DMBI	$1.9 \times 10\text{-}^{1}$	-426	3.5×10^{0}	11[b]	[14]

FBDPPV	N-DMBI	1.1×10^{1}	-126	18×10^{1}	28	[14]
FBDPPV	N-DMBI	6.0×10^{0}	-213	2.71×10^{1}	24[b]	[14]
FBDPPV	N-DMBI	4.5×10^{-1}	-658	1.91×10^{1}	11[b]	[14]
FBDPPV	N-DMBI	1.2×10^{1}	-131	2.1×10^{1}	31	[15]
FBDPPV	N-DMBI	1.5×10^{0}	-326	1.6×10^{1}	16[b]	[15]
FBDPPV	N-DMBI	6.1×10^{0}	-204	2.5×10^{1}	24[b]	[15]
ClBDPPV	TBAF	6.2×10^{-1}	-99	6.1×10^{-1}	25	[16]
ClBDPPV	TBAF	2.5×10^{-1}	-375	3.5×10^{0}	10[b]	[16]
BBL	TDAE	1.7×10^{0}	-60	6.1×10^{-1}	NA[a]	[11]
P(BTP-DPP)	$(RuCp^*mes)_2$	4.5×10^{-1}			27	[17]
P(PymPh)	NaNap	1.8×10^{1}	-16	4.8×10^{-1}	NA[a]	[18]
PC 61 BM	2-Cyc-DMBI-H	5.8×10^{-2}			11	[5]
PC 61 BM	$(2\text{-Cyc-DMBI})_2$	4.7×10^{-2}			10	[5]
PC 61 BM	$(2\text{-Fc-DMBI})_2$	1.9×10^{-3}			6	[5]
PC 61 BM	$(2\text{-Rc-DMBI})_2$	1.6×10^{-2}			11	[5]
C60	$(2\text{-Cyc-DMBI})_2$	1.2×10^{1}			26	[5]
C60	$(2\text{-Fc-DMBI})_2$	8.0×10^{-2}			20	[5]
C60	$(2\text{-Rc-DMBI})_2$	1.0×10^{-1}			18	[5]
C60	LCV	1.3×10^{-2}			6	[19]
C60	ACB	2.7×10^{-2}			5	[20]
PCBM	N-DMBI	1.9×10^{-3}			27	[21]
C60	$Cr_2(hpp)_4$	4.0×10^{0}			4	[22]
C60	$W_2(hpp)_4$	4.0×10^{0}			12	[22]
C60	AOB	6.0×10^{-1}	-188	2.1×10^{0}	34	[23]
C60	DMBI-POH	5.3×10^{0}	-161	1.3×10^{1}	39	[23]
C60	o-MeO-DMBI-I	5.5×10^{0}			14	[24]
PCBM	AOB	1.0×10^{-2}	-159	2.5×10^{-2}	33	[25]
PCBM	DMBI-POH	1.9×10^{0}	-124	2.9×10^{0}	41	[25]
PCBM	AOB+DMBI-POH	4.1×10^{0}	-187	1.4×10^{1}	33	[25]
PTEG-1	N-DMBI	2.1×10^{0}	-284	1.7×10^{1}	40	[26]
PCBM	N-DMBI	1.2×10^{-2}	-248	7.3×10^{-2}	30	[26]
PTEG-1	TEG-DMBI	1.8×10^{0}	-325	1.9×10^{1}	20	[27]
PTEG-1	N-DMBI	1.9×10^{0}	-291	1.6×10^{1}	40	[27]
PCBM	TBAI	5.6×10^{-3}			10	[28]

PCBM	TBAAcO	3.5×10^{-3}			20	[28]
PCBM	TBABr	3.1×10^{-3}			10	[28]
PCBM	TBAF	2.4×10^{-3}			10	[28]
PCBM	TBAOH	3.9×10^{-3}			10	[28]

[a] sequentially doped samples
[b] dopant molar fraction not at highest conductivity, but within specification (green area, Figure 1)

Determining the disorder parameter

The charge carrier density in the pristine polymer can be considered to be very low (cf. EPR spectrum). A constant charge carrier density is assumed over variable temperatures conductivity measurements, hence the activation energy of conductivity and charge carrier mobility should be equal. The measured activation energy is compared to the value to which the simulated activation energy of mobility converges at low density in Figure S3. The disorder parameter of the materials is then determined by identifying which line converges to the measured activation energy of the conductivity. In the case of an activation energy of 290 meV, a disorder parameter of 90 meV is found.

Determining charge carrier density

When the disorder parameter is determined from the pristine material, the activation energy of conductivity for the doped material can be measured. Assuming equal disorder parameters for the pristine and doped materials, the carrier density for the measured activation energy can then be estimated from Figure S3. The unit of charge carrier density is per hopping site volume in Figure S3, so to calculate the charge carrier density in SI units (or other preferred units), this carrier density should be multiplied by the density of states per unit volume. In this work, the density of states is estimated to be 10^{21} cm^{-3}.

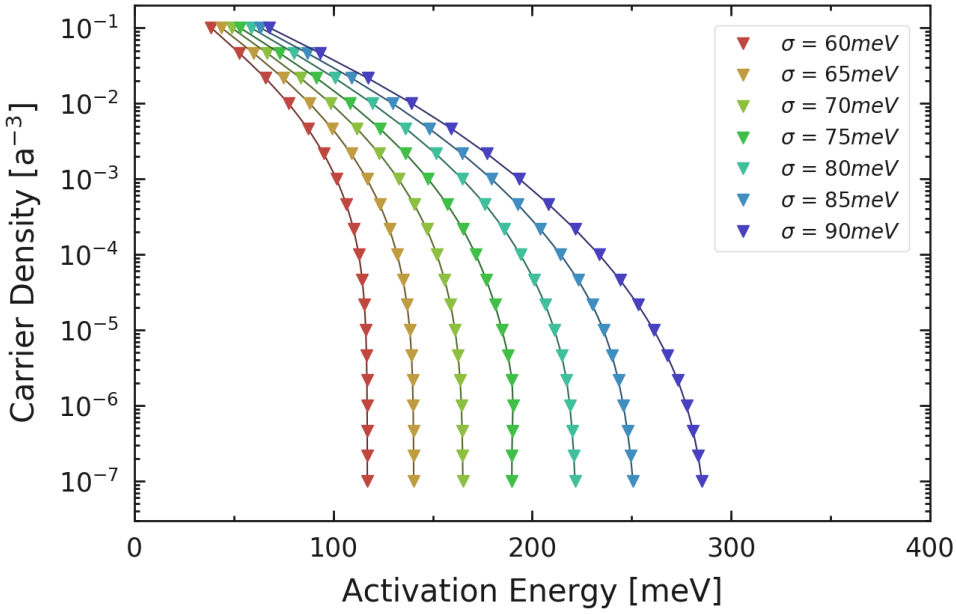

Figure S3. Results of activation energy fits to the charge carrier mobility calculated by the extended Gaussian disorder model using a temperature range of 260-300 K. Different disorder parameters (σ), result in different activation energies. The charge carrier density is expressed per effective hopping site volume.

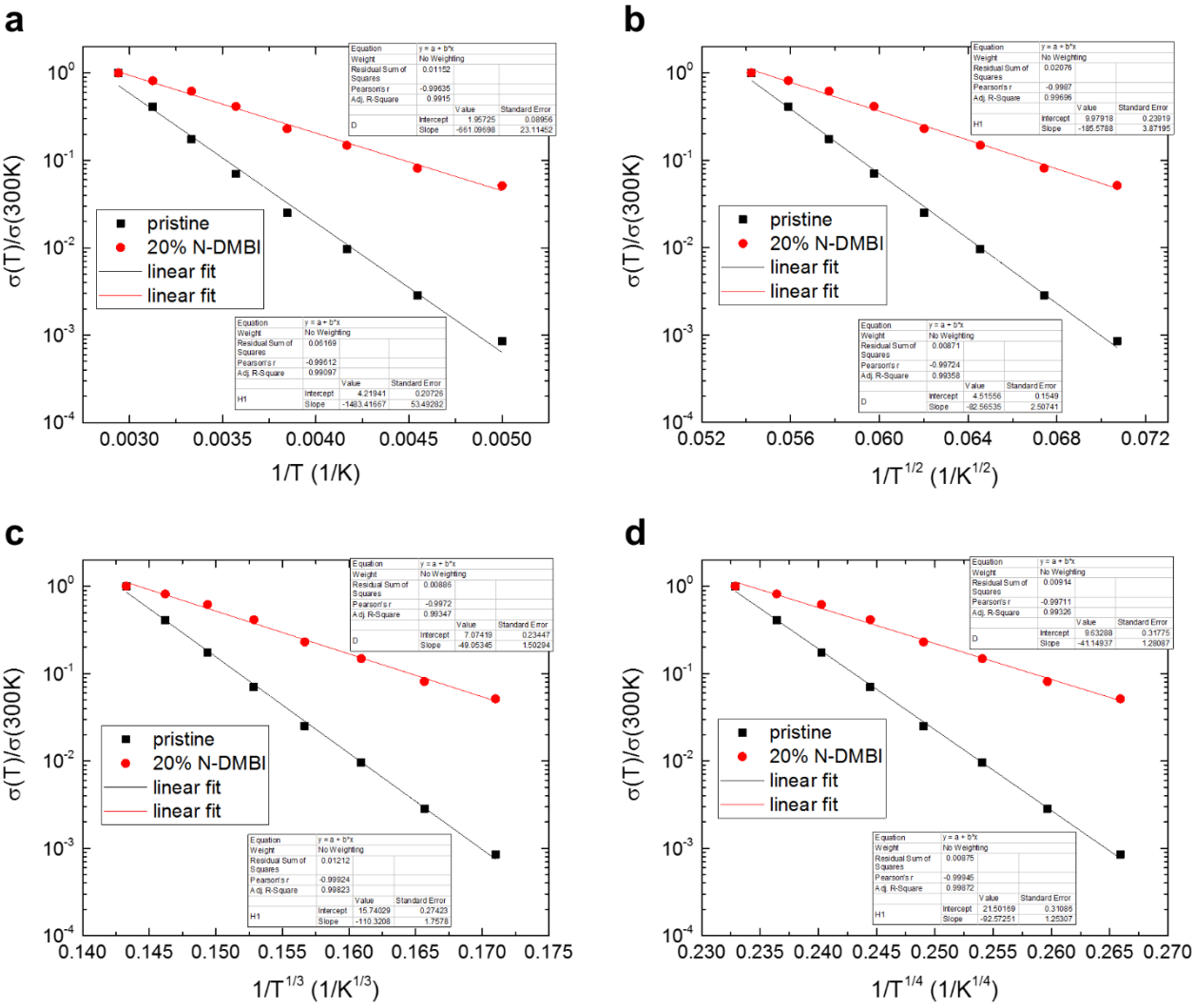

Figure S4. Fits to the variable temperature conductivity data of pristine p(gNDI-gT2) (black) and doped with 20 mol% N-DMBI (red) with $\log(\alpha) = \log(\sigma_0) - \left(\frac{1}{T}\right)^{\alpha}$, where σ_0 is a pre-exponential factor, and $\alpha = (1+d)^{-1}$. Different dimensionality exponents d were used in (a) $d = 0$ for variable range hopping, and (b) 1, (c) 2, and (d) 3 for 1-, 2-, and 3D variable range hopping.

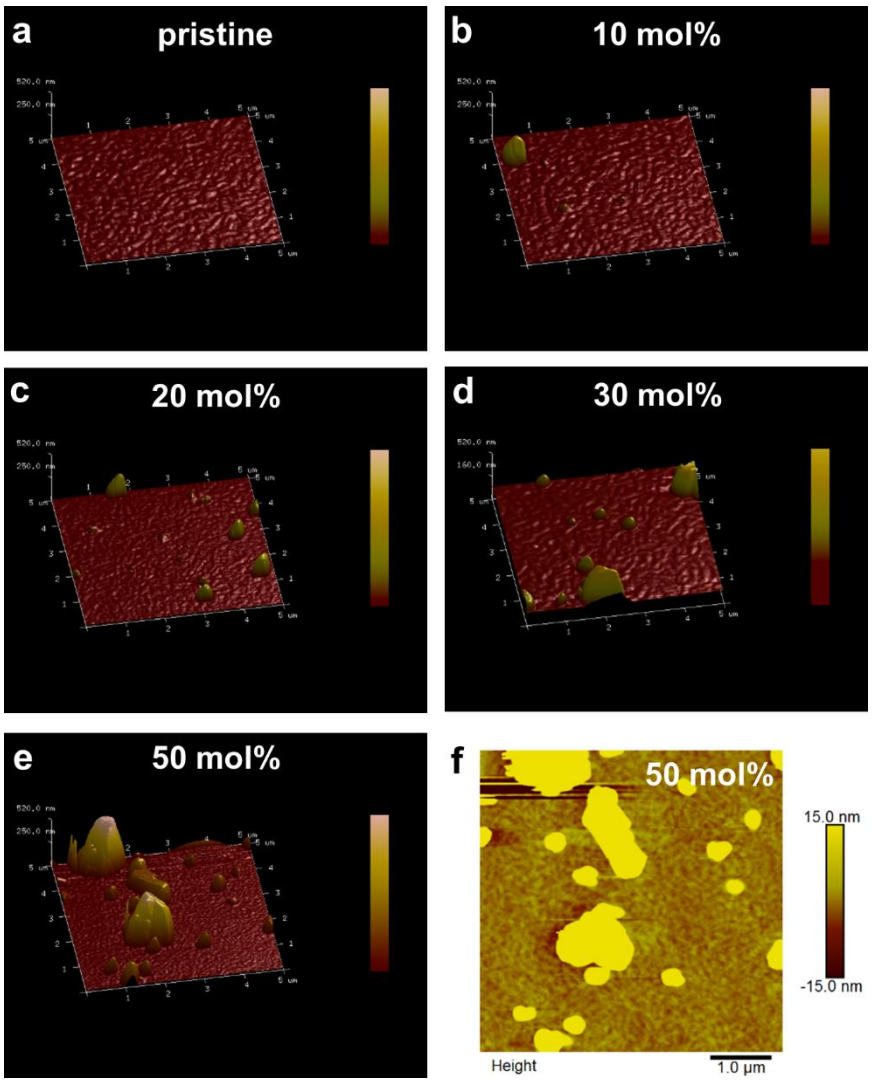

Figure S5. 3D topography images from AFM scans of (a) pristine p(gNDI-gT2) and doped with (b) 10 mol%, (c) 20 mol%, (d) 30 mol% and (e) 50 mol% N-DMBI. (f) AFM height image of p(gNDI-gT2) doped with 50 mol% N-DMBI (5 x 5 μm).

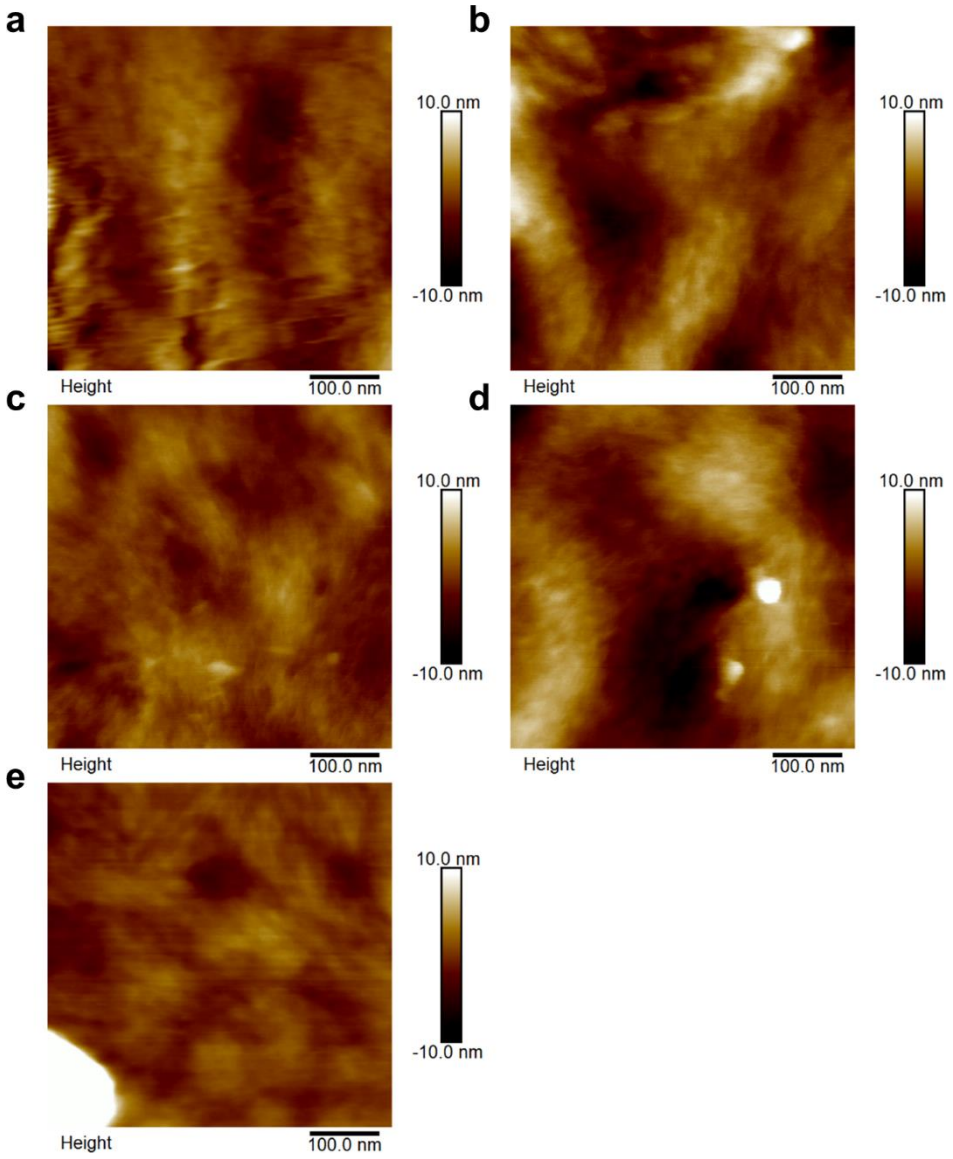

Figure S6. AFM height images of (a) pristine p(gNDI-gT2) and doped with (b) 10 mol%, (c) 20 mol%, (d) 30 mol% and (e) 50 mol% N-DMBI (0.5 x 0.5 μm).

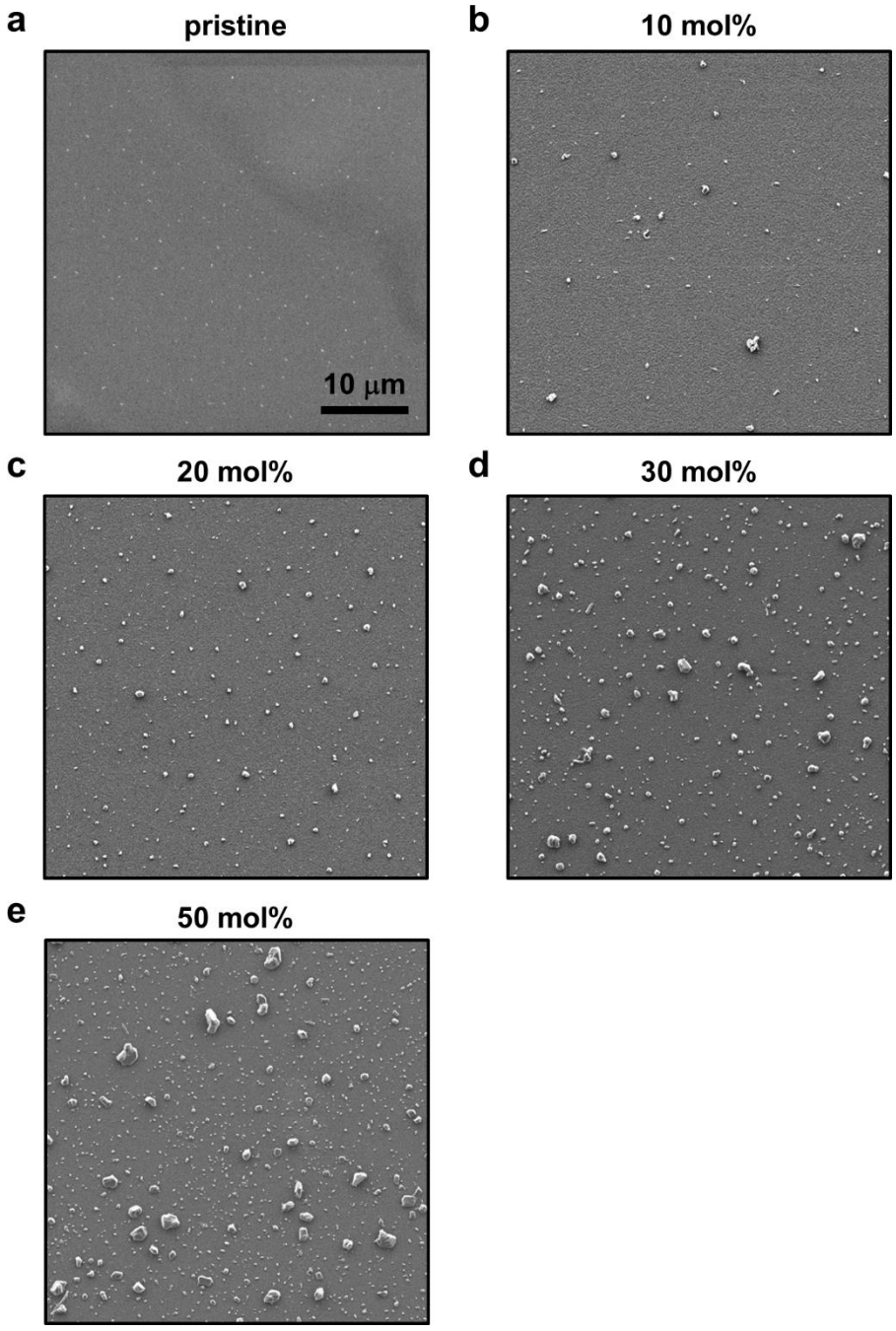

Figure S7. SEM images of (a) pristine p(gNDI-gT2) and doped with (b) 10 mol%, (c) 20 mol%, (d) 30 mol% and (e) 50 mol% N-DMBI (scale in (a) applies to all images).

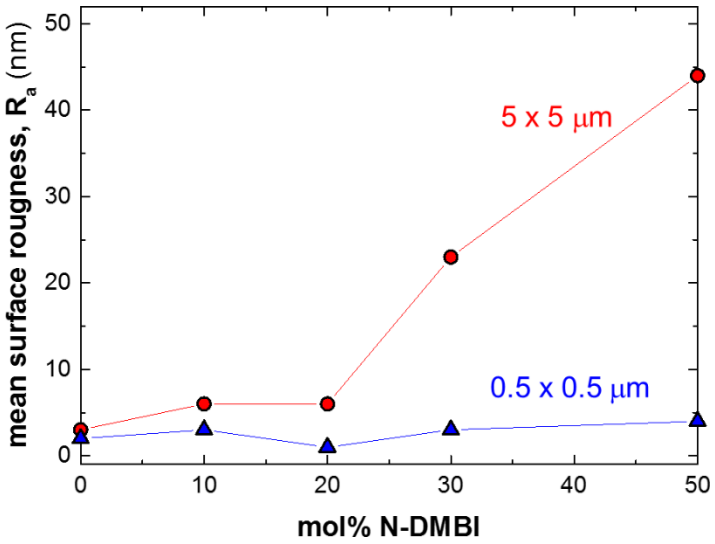

Figure S8. Mean surface roughness (R_a) extracted from AFM height images over a large surface area (5 × 5 μm) and over the area between the segregates (0.5 × 0.5 μm) at various dopant fractions. We note that the surface roughness changes only slightly from 2 nm for the pristine film to 6 nm after up to 20 mol% N-DMBI is added, but increases sharply for 30 mol% and more. Intriguingly, the surface roughness in the regions between the aggregates is not significantly affected by doping, even at higher doping fractions, which suggests that the nanostructure of the pristine polymer is largely maintained.

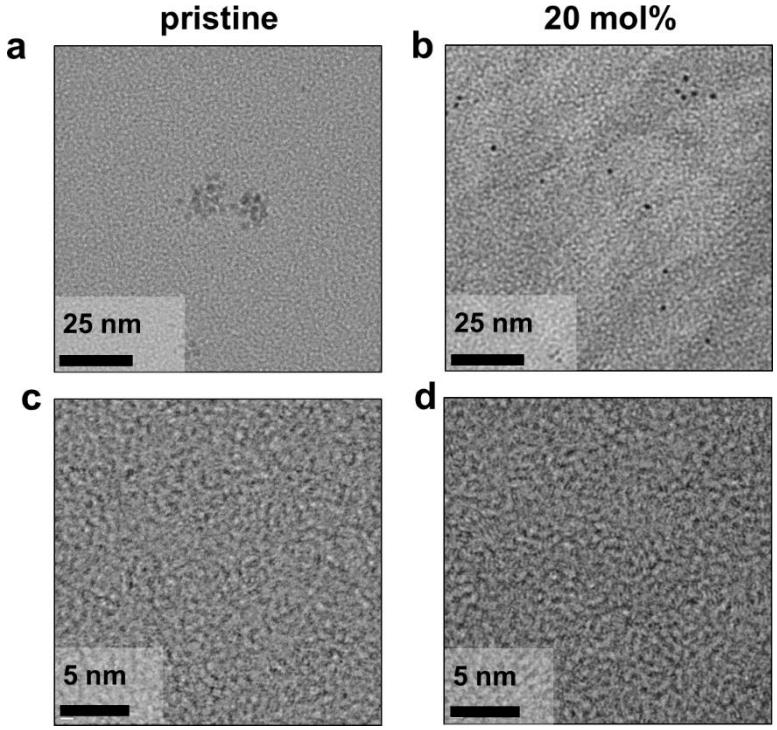

Figure S9. TEM images of (a,c) pristine p(gNDI-gT2) and (b,d) doped with 20 mol% N-DMBI.

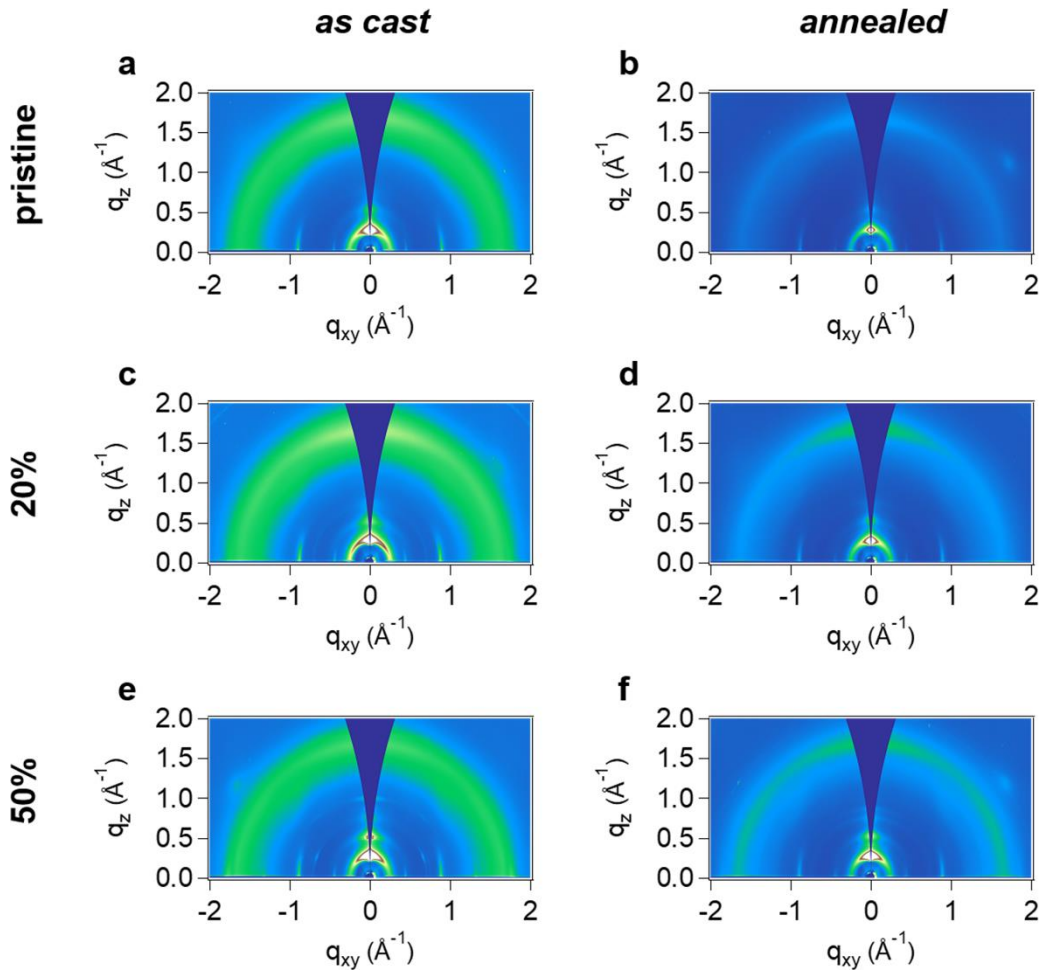

Figure S10. Grazing-incidence wide-angle X-ray scattering images for as cast films of (a) pristine p(gNDI-gT2), (c) 20 and (e) 50 mol% N-DMBI; and after annealing at 80 °C for 10 minutes, (b), (d), and (f), respectively.

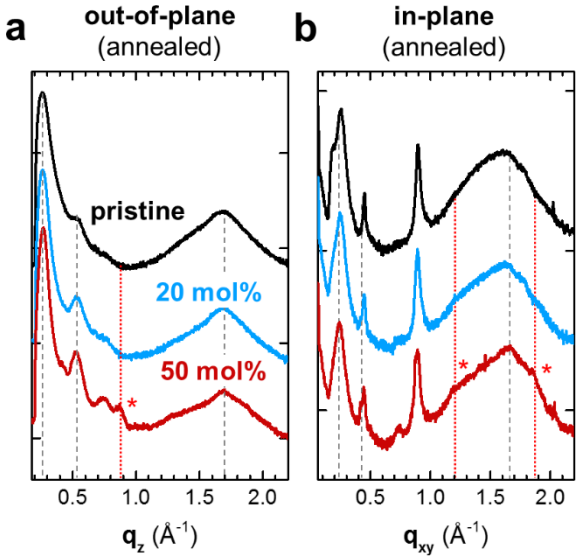

Figure S11. X-ray diffractograms of annealed films of pristine p(gNDI-gT2) and doped with 20 and 50 mol% obtained by integration along (a) the out-of-plane (q_z) and (b) in-plane (q_{xy}) direction. Annealing does not significantly alter the structure of the polymer, but leads to a reduction of the scattering peaks associated with doping, marked with an asterisk (*).

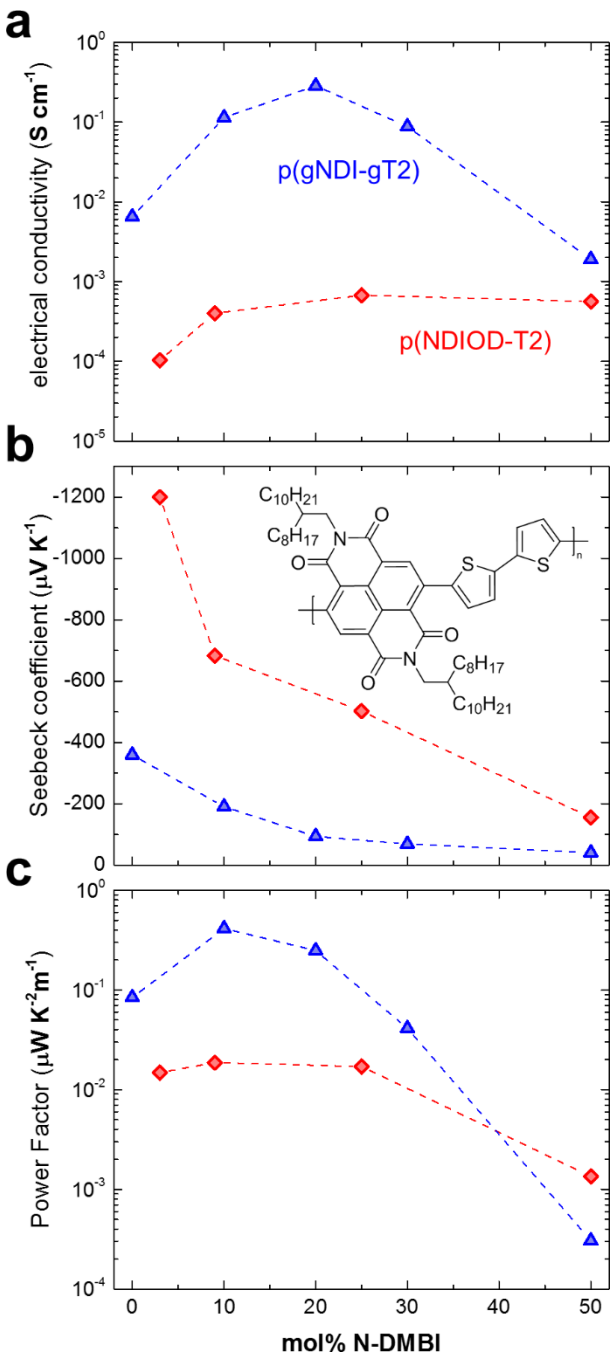

Figure S12. Electrical conductivity (a), Seebeck coefficient (b) and power factor (c) of p(gNDI-gT2) (blue) and p(NDI2OD-T2) (red) doped with N-DMBI; inset: chemical structure of p(NDI2OD-T2).

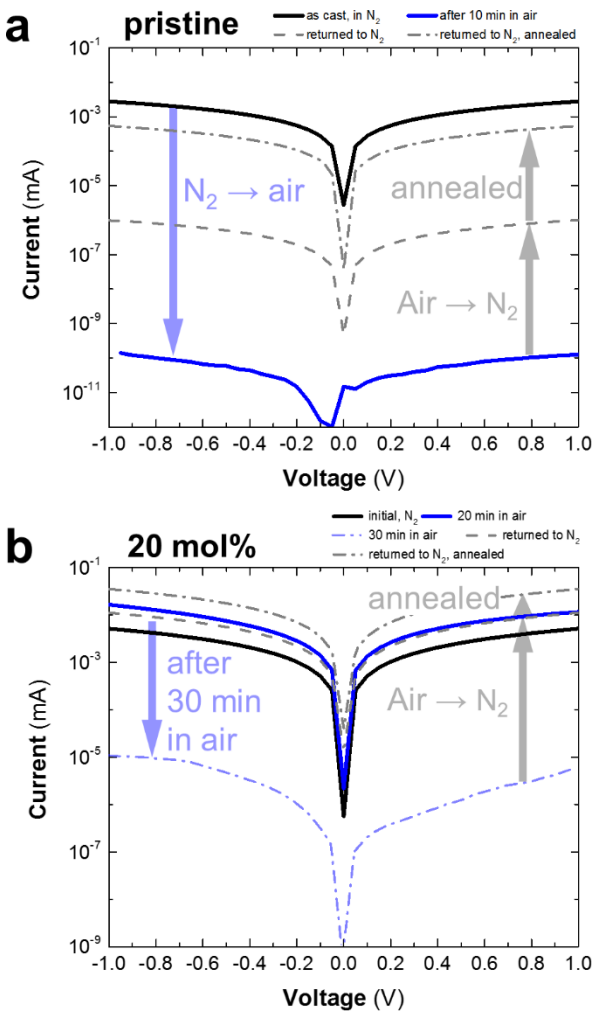

Figure S13. Air stability of the IV behavior of (a) pristine p(gNDI-gT2) and (b) doped with 20 mol% N-DMBI.

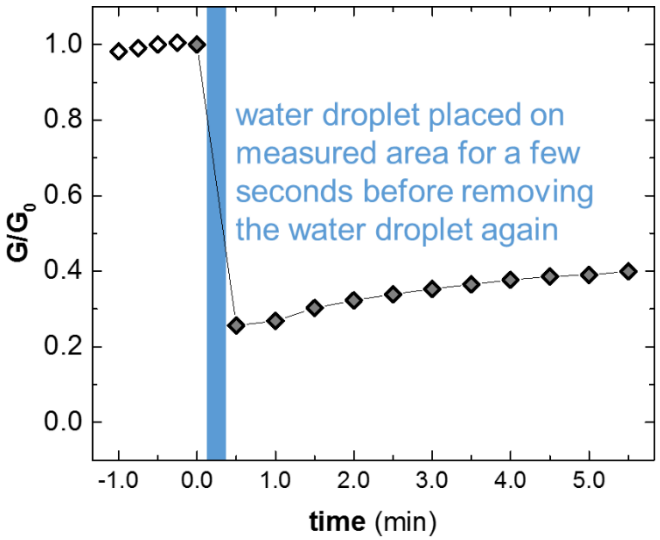

Figure S14. Relative conductance (G/G_0) before placing a water droplet on a film of p(gNDI-gT2) doped with 20 mol% N-DMBI for a few seconds and after removing the water droplet again.

References

(1) Giovannitti, A.; Nielsen, C. B.; Sbircea, D. T.; Inal, S.; Donahue, M.; Niazi, M. R.; Hanifi, D. A.; Amassian, A.; Malliaras, G. G.; Rivnay, J.; McCulloch, I. N-type Organic Electrochemical Transistors with Stability in Water. *Nat. Commun.* **2016,** *7*, 13066.

(2) Ilavsky, J. Nika: Software for Two-Dimensional Data Reduction. *J. Appl. Crystallogr.* **2012,** *45*, 324-328.

(3) Oosterhout, S. D.; Savikhin, V.; Zhang, J.; Zhang, Y.; Burgers, M. A.; Marder, S. R.; Bazan, G. C.; Toney, M. F. Mixing Behavior in Small Molecule:Fullerene Organic Photovoltaics. *Chem. Mater.* **2017,** *29*, 3062-3069.

(4) Cho, N.; Yip, H.-L.; Davies, J. A.; Kazarinoff, P. D.; Zeigler, D. F.; Durban, M. M.; Segawa, Y.; O'Malley, K. M.; Luscombe, C. K.; Jen, A. K. Y. In-situ Crosslinking and n-Doping of Semiconducting Polymers and Their Application as Efficient Electron-Transporting Materials in Inverted Polymer Solar Cells. *Adv. Energy Mater.* **2011,** *1*, 1148-1153.

(5) Naab, B. D.; Zhang, S.; Vandewal, K.; Salleo, A.; Barlow, S.; Marder, S. R.; Bao, Z. Effective Solution- and Vacuum-Processed n-Doping by Dimers of Benzimidazoline Radicals. *Adv. Mater.* **2014,** *26*, 4268-72.

(6) Schlitz, R. A.; Brunetti, F. G.; Glaudell, A. M.; Miller, P. L.; Brady, M. A.; Takacs, C. J.; Hawker, C. J.; Chabinyc, M. L. Solubility-Limited Extrinsic n-Type Doping of a High Electron Mobility Polymer for Thermoelectric Applications. *Adv. Mater.* **2014,** *26*, 2825-30.

(7) Liang, Y.; Chen, Z.; Jing, Y.; Rong, Y.; Facchetti, A.; Yao, Y. Heavily n-Dopable π-Conjugated Redox Polymers with Ultrafast Energy Storage Capability. *J. Am. Chem. Soc.* **2015,** *137*, 4956-9.

(8) Naab, B. D.; Gu, X.; Kurosawa, T.; To, J. W. F.; Salleo, A.; Bao, Z. Role of Polymer Structure on the Conductivity of N-Doped Polymers. *Adv. Electron. Mater.* **2016,** *2*, 1600004.

(9) Zhang, Y.; Phan, H.; Zhou, H.; Zhang, X.; Zhou, J.; Moudgil, K.; Barlow, S.; Marder, S. R.; Facchetti, A.; Nguyen, T.-Q. Electron Transport and Nanomorphology in Solution-Processed Polymeric Semiconductor n-Doped with an Air-Stable Organometallic Dimer. *Adv. Electron. Mater.* **2017,** *3*, 1600546.

(10) Higgins, A.; Mohapatra, S. K.; Barlow, S.; Marder, S. R.; Kahn, A. Dopant Controlled Trap-Filling and Conductivity Enhancement in an Electron-Transport Polymer. *Appl. Phys. Lett.* **2015,** *106*, 163301.

(11) Wang, S.; Sun, H.; Ail, U.; Vagin, M.; Persson, P. O.; Andreasen, J. W.; Thiel, W.; Berggren, M.; Crispin, X.; Fazzi, D.; Fabiano, S. Thermoelectric Properties of Solution-Processed n-Doped Ladder-Type Conducting Polymers. *Adv. Mater.* **2016,** *28*, 10764-10771.

(12) Madan, D.; Zhao, X.; Ireland, R. M.; Xiao, D.; Katz, H. E. Conductivity and Power Factor Enhancement of n-Type Semiconducting Polymers using Sodium Silica Gel Dopant. *APL Mater.* **2017,** *5*, 086106.

(13) Wang, Y.; Nakano, M.; Michinobu, T.; Kiyota, Y.; Mori, T.; Takimiya, K. Naphthodithiophenediimide–Benzobisthiadiazole-Based Polymers: Versatile n-Type Materials for Field-Effect Transistors and Thermoelectric Devices. *Macromolecules* **2017,** *50*, 857-864.

(14) Shi, K.; Zhang, F.; Di, C. A.; Yan, T. W.; Zou, Y.; Zhou, X.; Zhu, D.; Wang, J. Y.; Pei, J. Toward High Performance n-Type Thermoelectric Materials by Rational Modification of BDPPV Backbones. *J. Am. Chem. Soc.* **2015,** *137*, 6979-82.

(15) Ma, W.; Shi, K.; Wu, Y.; Lu, Z. Y.; Liu, H. Y.; Wang, J. Y.; Pei, J. Enhanced Molecular Packing of a Conjugated Polymer with High Organic Thermoelectric Power Factor. *ACS Appl. Mater. Interfaces* **2016,** *8*, 24737-43.

(16) Zhao, X.; Madan, D.; Cheng, Y.; Zhou, J.; Li, H.; Thon, S. M.; Bragg, A. E.; DeCoster, M. E.; Hopkins, P. E.; Katz, H. E. High Conductivity and Electron-Transfer Validation in an n-Type Fluoride-Anion-Doped Polymer for Thermoelectrics in Air. *Adv. Mater.* **2017,** *29*, 1606928.

(17) Perry, E. E.; Chiu, C.-Y.; Moudgil, K.; Schlitz, R. A.; Takacs, C. J.; O'Hara, K. A.; Labram, J. G.; Glaudell, A. M.; Sherman, J. B.; Barlow, S.; Hawker, C. J.; Marder, S. R.; Chabinyc, M. L. High Conductivity in a Nonplanar n-Doped Ambipolar Semiconducting Polymer. *Chem. Mater.* **2017,** *29*, 9742-9750.

(18) Hwang, S.; Potscavage, W. J.; Yang, Y. S.; Park, I. S.; Matsushima, T.; Adachi, C. Solution-Processed Organic Thermoelectric Materials Exhibiting Doping-Concentration-Dependent Polarity. *Phys. Chem. Chem. Phys.* **2016,** *18*, 29199-29207.

(19) Li, F.; Werner, A.; Pfeiffer, M.; Leo, K.; Liu, X. Leuco Crystal Violet as a Dopant for n-Doping of Organic Thin Films of Fullerene C60. *J. Phys. Chem. B* **2004,** *108*, 17076-17082.

(20) Li, F.; Pfeiffer, M.; Werner, A.; Harada, K.; Leo, K.; Hayashi, N.; Seki, K.; Liu, X.; Dang, X.-D. Acridine Orange Base as a Dopant for n-Doping of C60 Thin Films. *J. Appl. Phys.* **2006,** *100*, 023716.

(21) Wei, P.; Oh, J. H.; Dong, G.; Bao, Z. Use of a 1H-Benzoimidazole Derivative as an n-Type Dopant and to Enable Air-Stable Solution-Processed n-Channel Organic Thin-Film Transistors. *J. Am. Chem. Soc.* **2010,** *132*, 8852-3.

(22) Menke, T.; Ray, D.; Meiss, J.; Leo, K.; Riede, M. In-Situ Conductivity and Seebeck Measurements of Highly Efficient n-Dopants in Fullerene C60. *Appl. Phys. Lett.* **2012,** *100*, 093304.

(23) Menke, T.; Wei, P.; Ray, D.; Kleemann, H.; Naab, B. D.; Bao, Z.; Leo, K.; Riede, M. A Comparison of Two Air-Stable Molecular n-Dopants for C60. *Org. Electron.* **2012,** *13*, 3319-3325.

(24) Wei, P.; Menke, T.; Naab, B. D.; Leo, K.; Riede, M.; Bao, Z. 2-(2-Methoxyphenyl)-1,3-dimethyl-1H-benzoimidazol-3-ium Iodide as a New Air-Stable n-Type Dopant for Vacuum-Processed Organic Semiconductor Thin Films. *J. Am. Chem. Soc.* **2012,** *134*, 3999-4002.

(25) Gao, F.; Liu, Y.; Xiong, Y.; Wu, P.; Hu, B.; Xu, L. Fabricate Organic Thermoelectric Modules use Modified PCBM and PEDOT:PSS Materials. *Front. Optoelectron.* **2017,** *10*, 117-123.

(26) Liu, J.; Qiu, L.; Portale, G.; Koopmans, M.; Ten Brink, G.; Hummelen, J. C.; Koster, L. J. A. N-Type Organic Thermoelectrics: Improved Power Factor by Tailoring Host-Dopant Miscibility. *Adv. Mater.* **2017,** *29*, 1701641.

(27) Qiu, L.; Liu, J.; Alessandri, R.; Qiu, X.; Koopmans, M.; Havenith, Remco W. A.; Marrink, S. J.; Chiechi, R. C.; Anton Koster, L. J.; Hummelen, J. C. Enhancing Doping Efficiency by Improving Host-Dopant Miscibility for Fullerene-Based n-Type Thermoelectrics. *J. Mater. Chem. A* **2017,** *5*, 21234-21241.

(28) Li, C. Z.; Chueh, C. C.; Ding, F.; Yip, H. L.; Liang, P. W.; Li, X.; Jen, A. K. Doping of Fullerenes via Anion-Induced Electron Transfer and its Implication for Surfactant Facilitated High Performance Polymer Solar Cells. *Adv. Mater.* **2013,** *25*, 4425-30.